HOST-PATHOGEN INTERACTIONS

The microRNA miR-485 targets host and influenza virus transcripts to regulate antiviral immunity and restrict viral replication

Harshad Ingle,[1]* Sushil Kumar,[1]* Ashwin Ashok Raut,[2] Anamika Mishra,[2] Diwakar Dattatraya Kulkarni,[2] Takeshi Kameyama,[3] Akinori Takaoka,[3] Shizuo Akira,[4] Himanshu Kumar[1,4]†

MicroRNAs (miRNAs) are small noncoding RNAs that are responsible for dynamic changes in gene expression, and some regulate innate antiviral responses. Retinoic acid–inducible gene I (RIG-I) is a cytosolic sensor of viral RNA; RIG-I activation induces an antiviral immune response. We found that miR-485 of the host was produced in response to viral infection and targeted *RIG-I* mRNA for degradation, which led to suppression of the antiviral response and enhanced viral replication. Thus, inhibition of the expression of *mir-485* markedly reduced the replication of Newcastle disease virus (NDV) and the H5N1 strain of influenza virus in mammalian cells. Unexpectedly, miR-485 also bound to the H5N1 gene *PB1* (which encodes an RNA polymerase required for viral replication) in a sequence-specific manner, thereby inhibiting replication of the H5N1 virus. Furthermore, miR-485 exhibited bispecificity, targeting *RIG-I* in cells with a low abundance of H5N1 virus and targeting *PB1* in cells with increased amounts of the H5N1 virus. These findings highlight the dual role of miR-485 in preventing spurious activation of antiviral signaling and restricting influenza virus infection.

INTRODUCTION

The mammalian innate immune system consists of an array of pattern recognition receptors (PRRs) that sense conserved signature microbial molecules known as pathogen-associated molecular patterns (PAMPs) (*1*). Retinoic acid–inducible gene I (RIG-I)–like receptors (RLRs) sense viral RNA in the cytosol. The RLRs RIG-I (which is encoded by *DDX58*, hereafter referred to as *RIG-I*) and melanoma differentiation–associated gene 5 (MDA5) are recruited to IPS-1 [interferon-β (IFN-β) promoter stimulator 1; also known as Cardif, MAVS, or VISA], which is localized to the outer mitochondrial membrane, to initiate a signaling cascade through the activation of the transcription factors IFN regulatory factor 3 (IRF3), IRF7, and nuclear factor κB (NF-κB). This cascade leads to the induction of an array of genes whose products exert pleiotropic effects on viral replication (*2*–*5*). This complex mechanism of antiviral signaling is balanced by regulating the activation of RIG-I or the key intermediates of the pathway. Posttranslational mechanisms, such as ubiquitylation or phosphorylation, which provide the activation signal for RIG-I, have been well characterized; these mechanisms are targeted by viruses to delay or evade the immune response (*6*–*8*). There is an increasing amount of evidence that microRNAs (miRNAs) play a role in fine-tuning the antiviral immune response by targeting signaling components of the RLR pathway (*9*–*11*); however, the posttranscriptional regulation of RLR sensors, especially RIG-I, remains elusive.

miRNAs are small noncoding RNAs that contribute to the regulation of key cellular processes by binding to the 3′ untranslated regions (3′UTRs) of their target genes, which inhibits their transcription and protein synthesis (*12*–*14*). miRNA profiling studies have identified miRNAs whose expression is induced after cells are infected by RNA viruses and that modulate the antiviral response by targeting immune signaling pathways (*15*–*17*). Additionally, miRNAs targeting the genomes of RNA viruses have also been identified (*18*, *19*). Nevertheless, to our knowledge, there are no reports of the same miRNA targeting both the RLR sensor and the viral genome. Such a dual role for host miRNAs in regulating host antiviral proteins to maintain homeostasis (that is, preventing unwanted activation of the antiviral response) and in targeting viral RNAs to inhibit viral replication could lead to the identification of unique miRNA–host mRNA and miRNA–viral RNA relationships.

Here, we identified and characterized miR-485 as an miRNA whose expression was induced by infection with RNA viruses, including Newcastle disease virus (NDV) and the influenza virus, or by transfection of cells, including human peripheral blood mononuclear cells (PBMCs), with polyinosinic-polycytidylic acid [poly(I:C)], a synthetic mimetic of viral double-stranded RNA (dsRNA). miR-485 directly targeted the 3′UTR of the gene encoding RIG-I. Ectopic expression of miR-485 in human and mouse cells impaired the RIG-I–dependent antiviral response, resulting in an increased viral load. We found that miR-485 formed a stable complex with the human Argonaute 2 (Ago2) protein and was recruited to the *RIG-I* transcript upon viral infection.

The influenza A virus (IAV) contains a segmented genome that is sensed by endosome-localized Toll-like receptor 3 (TLR3), TLR7, and TLR8, as well as by the cytosolic sensor RIG-I, to induce appropriate innate immune responses (*20*–*22*). The IAV genome encodes the structural proteins hemagglutinin (HA) and neuraminidase (NA). The genome can undergo genetic reassortment, giving rise to new subtypes and enabling the virus to infect a wide range of hosts. In contrast, the viral ribonucleoprotein (RNP), which consists of the polymerase proteins PB1, PB2, and PA, is more conserved across different strains (*23*). Additionally, we showed that miR-485 also bound to a conserved region in the *PB1* gene of IAV, thereby suppressing viral replication.

[1]Laboratory of Immunology, Department of Biological Sciences, Indian Institute of Science Education and Research, Bhopal 462066, India. [2]Pathogenomics Lab, OIE Reference Lab for Avian Influenza, ICAR-National Institute of High Security Animal Diseases, Bhopal 462022, India. [3]Division of Signaling in Cancer and Immunology, Institute for Genetic Medicine, Hokkaido University, Sapporo 060-0815, Japan. [4]Laboratory of Host Defense, WPI Immunology Frontier Research Centre, Osaka University, Osaka 565-0871, Japan.
*These authors contributed equally to this work.
†Corresponding author. E-mail: hkumar@iiserb.ac.in

Both of these mechanisms were dependent on the magnitude of infection. At low doses of IAV, miR-485 targeted the RIG-I transcript; however, when an increased amount of IAV was present, miR-485 switched to targeting PB1, and the cells became resistant to IAV infection. We propose a model for the bispecificity of miR-485 toward both RIG-I and PB1 and provide a basic understanding of the involvement of host miRNA in the maintenance of homeostasis and the restriction of IAV infections.

RESULTS

mir-485 expression is induced by viral infection and intracellular delivery of poly(I:C)

To identify the miRNAs involved in regulating antiviral signaling pathways, we performed microarray-based miRNA profiling in human embryonic kidney (HEK) 293T cells infected with live NDV (LaSota strain) at a multiplicity of infection (MOI) of 1 for 6 hours. We selected miRNAs that were increased in abundance more than 1.1-fold (table S1). This low threshold was chosen because minor changes in miRNA abundance can result in substantial phenotypic variations (*14*). Using the KEGG (Kyoto Encyclopedia of Genes and Genomes) pathway analysis database, we identified three major antiviral pathways that were targeted by the miRNAs that were increased in abundance (Fig. 1A). Next, we designed a screening pipeline and applied this to the selected miRNAs (Fig. 1B). Those miRNAs that were decreased in abundance in response to NDV infection were also subjected to the screening pipeline to further eliminate any false negatives. Four miRNAs (miR-146a, miR-205, miR-485, and miR-125a) were predicted to have the highest scores for targeting RIG-I, but not the other RNA sensors, such as MDA5, TLR3, TLR7, TLR8, or TLR9, on the basis of the scoring parameters of the in silico tools (Fig. 1C).

For standardization of viral infection, human small airway epithelial cells (SAECs) (fig. S1, A to C), A549 cells (fig. S1, D to F), HEK 293T cells (fig. S1, G to K), and human PBMCs (fig. S1L) were infected with H5N1 or NDV. Similarly, both HEK 293T cells (fig. S2, A and B) and MCF7 cells (fig. S2, C and D) were transfected with poly(I:C). We further analyzed the expression of the four selected miRNAs in different cell lines and primary cells (such as human PBMCs) after infection with NDV or H5N1 or transfection with poly(I:C). NDV induced the expression of *mir-485*, but not *mir-125a*, *mir-205*, or *mir-146a* in HEK 293T cells and PBMCs (Fig. 1, D and E). Similar results were observed in SAECs and A549 cells infected with H5N1 (Fig. 1, F and G). THP1, MCF7, HEK 293T, and HeLa cells transfected with poly(I:C) also exhibited a specific increase in the expression of *mir-485* (Fig. 1, H to K).

RIG-I–mediated signaling induces the production of type I IFNs, proinflammatory cytokines, and a wide range of secondary antiviral effectors. Therefore, we tested whether the induction of miR-485 expression was dependent on the type I IFNs that were secreted in response to viral infection. However, when HEK 293T cells were treated with IFN-β, the abundance of miR-485 was unchanged (Fig. 1L, left), whereas the IFN-inducible gene *RIG-I* showed increased expression (Fig. 1L, right). One of the key aspects of the miRNA-mediated regulation of target genes depends on the relative proportion of the host cell miRNA pool that a given miRNA represents. To investigate the change in the abundance of miR-485, we infected HEK 293T cells with NDV and calculated the miR-485 copy number. We found that there was a steady increase in miR-485 abundance, copy number, and relative proportion of the host cell miRNA pool upon NDV infection (fig. S3, A to C).

To gain insights into the increased expression of miR-485, we scanned the upstream region of the *mir-485* gene for putative transcription factor–binding sites with the TRANSFAC, F-Match, and Alibaba 2.0 programs. These programs predicted an upstream region of 1.8 kb that contained binding motifs for a number of mammalian transcription factors; hence, this region was cloned into the pGL3 basic luciferase reporter vector (Fig. 1M). We found that there was a dose-dependent increase in miR-485 promoter activity in HEK 293T cells in response to NDV infection (Fig. 1N). However, both IFN-β and tumor necrosis factor–α (TNF-α) failed to induce miR-485 promoter activity, although both cytokines induced the IFN-stimulated response element (ISRE) and NF-κB promoters (Fig. 1, N and O). These results suggest that miR-485 expression is specifically induced in response to viral infection in a manner that is not directly dependent on type I IFNs or proinflammatory cytokines.

miR-485 directly targets the 3′UTR of RIG-I

The basal amount of the RIG-I protein senses viral nucleic acids in the cytosol and induces the production of type I IFNs. In turn, these IFNs increase the expression of a group of genes termed the IFN-stimulatory genes (ISGs), including the gene encoding RIG-I. Thus, the expression of *RIG-I* increases by a positive feedback system that can be inhibited by miR-485. Through bioinformatics tools such as TargetScan and miRanda, we identified two target sites of miR-485 in the 3′UTR of *RIG-I* (at positions 213 and 1784) (Fig. 2A), and these target sites are conserved in various organisms (fig. S4A). Furthermore, we scanned the 3′UTR of *RIG-I* for RNA binding protein sites with the iCLIP database and found a binding site for the Ago2 protein, which is the key component of the miRNA-mediated gene silencing complex (fig. S4B). The full-length 3′UTR of *RIG-I* was subcloned upstream of the luciferase reporter gene in the pMIR-Report vector. Binding of miR-485 to the RIG-I 3′UTR would thus reduce the expression of the luciferase gene. To overexpress miR-485, the sequence encoding miR-485 was subcloned into the plasmid pMIR-Report after removal of the luciferase construct, and is hereafter referred to as p485. Through luciferase reporter assays, we found a statistically significant, dose-dependent suppression of luciferase activity by p485 (Fig. 2B, left). Similar results were obtained with the miR-485 mimic (Fig. 2B, right); however, a mimic of an unrelated miRNA, miR-1, which is expressed in muscles, did not cause any reduction in luciferase activity. In contrast, introducing a mutation that disrupted the miR-485 seed sequence completely abrogated its ability to inhibit luciferase activity (Fig. 2C). Furthermore, the ectopic expression of miR-485 followed by infection with H5N1 or NDV markedly reduced the abundance of *RIG-I* mRNA in HEK 293T and HeLa cells (Fig. 2, D and E). Moreover, the amount of *RIG-I* mRNA was not reduced when cells expressing anti–miR-485 were infected with NDV (fig. S4C); however, anti–miR-125a, anti–miR-205, and anti–miR-146a had no substantial effect on the expression of *RIG-I* in NDV-infected HEK 293T cells (fig. S4D). Similar results were obtained from experiments in which HEK 293T and MCF7 cells were transfected with poly(I:C) in the presence of miR-485 (fig. S4E).

Next, we tested the role of miR-485 on primary human and mouse cells. We found that the abundance of *RIG-I* mRNA was markedly reduced in human PBMCs and granulocyte macrophage colony-stimulating factor (GM-CSF)–treated mouse bone marrow–derived dendritic cells (BMDCs) that were transfected with the miR-485 mimic and then were infected with NDV (Fig. 2F). Similar reductions in *RIG-I* mRNA abundance were observed in human PBMCs, mouse BMDCs, and human SAECs that were infected with H5N1 virus after having been transfected with the miR-485 mimic (Fig. 2G and fig. S4F). This reduction in *RIG-I* mRNA abundance was abrogated in the presence of anti–miR-485 in human PBMCs infected with H5N1 virus (fig. S4G). In addition, miR-485 modestly reduced the abundance of MDA5 mRNA in HEK 293T cells that were infected with H5N1 or NDV viruses or transfected with poly(I:C)

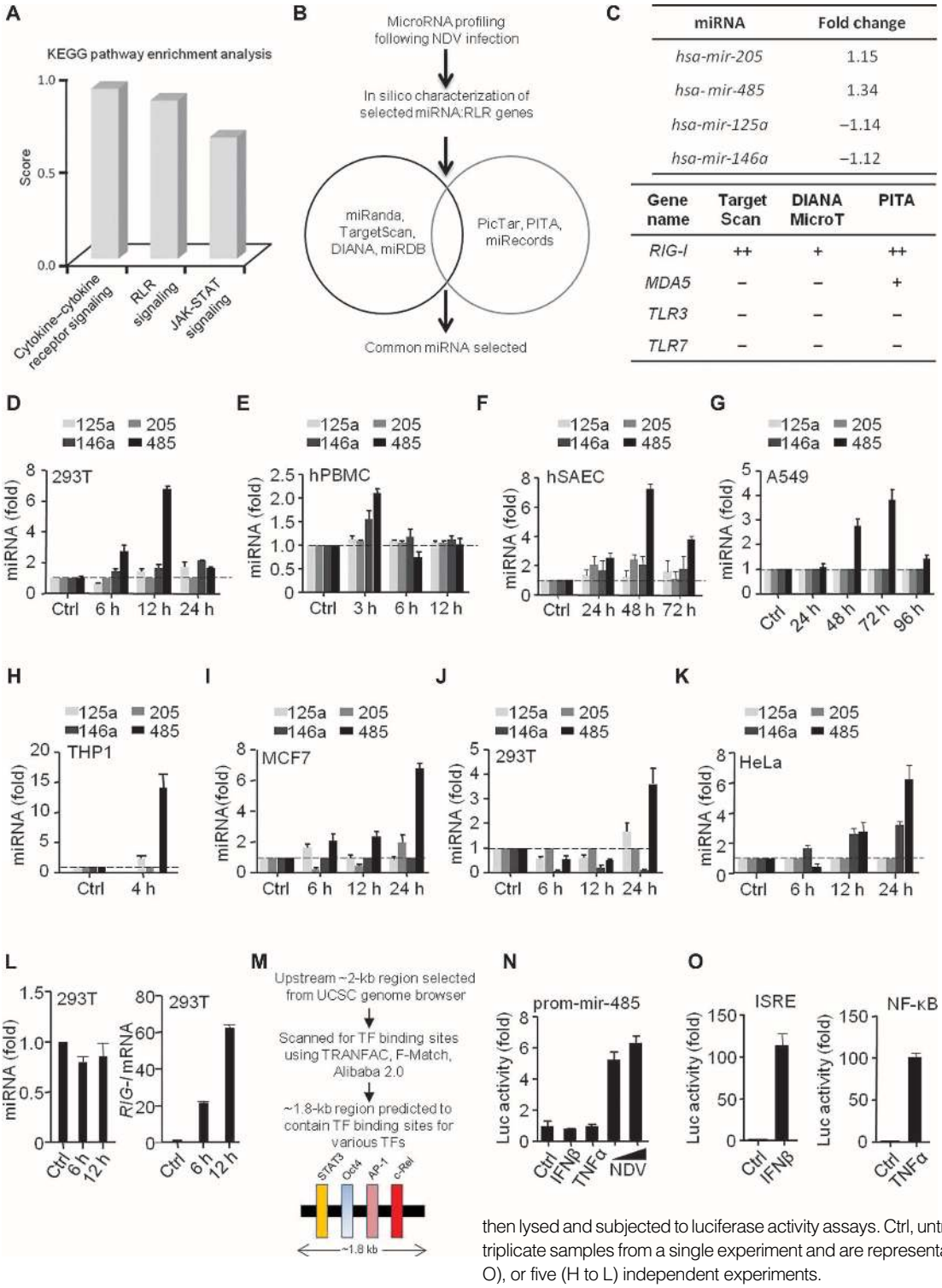

Fig. 1. Viral infection and transfection with poly(I:C) enhances the expression of *miR-485*. (**A**) KEGG pathway enrichment analysis of the miRNAs that were increased >1.1-fold in abundance in HEK 293T cells upon NDV infection. (**B**) Screening pipeline used for identifying miRNA target genes based on the indicated algorithms. (**C**) List of the candidate miRNAs with their abundance selected after screening with the indicated algorithms. (**D** to **K**) Quantification [as determined by quantitative reverse transcription polymerase chain reaction (qRT-PCR) analysis] of the fold changes in the abundances of miR-125a, miR-146a, miR-205, and miR-485 at the indicated times after NDV infection of HEK 293T cells (D) and human PBMCs (E); H5N1 infection (at an MOI of 1.0) of human SAECs (G) and A549 cells (H); and transfection of THP1 cells (H), MCF7 cells (I), HEK 293T cells (J), and HeLa cells (K) with poly(I:C) (10 μg/ml). The horizontal line represents basal abundance. (**L**) Quantification of the abundances of miR-485 (left) and *RIG-I* mRNA (right) in HEK 293T cells pretreated with recombinant human IFN-β (rhuIFN-β; 500 U/ml) for the indicated times. (**M**) Scheme for the in silico identification of the *mir-485* promoter. (**N** and **O**) HEK 293T cells were transfected with the miR-485-promoter construct and then were stimulated with rhuIFN-β or TNF-α for 12 hours or were infected with NDV at an MOI of 1 or 10 for 6 hours. Cells were then lysed and subjected to luciferase activity assays. Ctrl, untreated. Data are means ± SEM of triplicate samples from a single experiment and are representative of two (D to G), three (N and O), or five (H to L) independent experiments.

(fig. S5). Furthermore, we generated HEK 293T cells that stably expressed miR-485, hereafter referred to as H485 cells, and tested their expression of *mir-485* (Fig. 2H, left). H485 cells exhibited reductions in the abundances of both *RIG-I* mRNA and RIG-I protein in response to transfection with poly(I:C) compared to those in similarly treated HEK 293T cells (Fig. 2H, right and top). Moreover, the miR-485 mimic reduced the abundance of *RIG-I* mRNA in HEK 293T cells subsequently infected with NDV, whereas anti–miR-485 had the opposite effect (Fig. 2I).

Finally, to determine whether miR-485 regulated RIG-I transcriptionally or posttranscriptionally, we performed an RNA immunoprecipitation

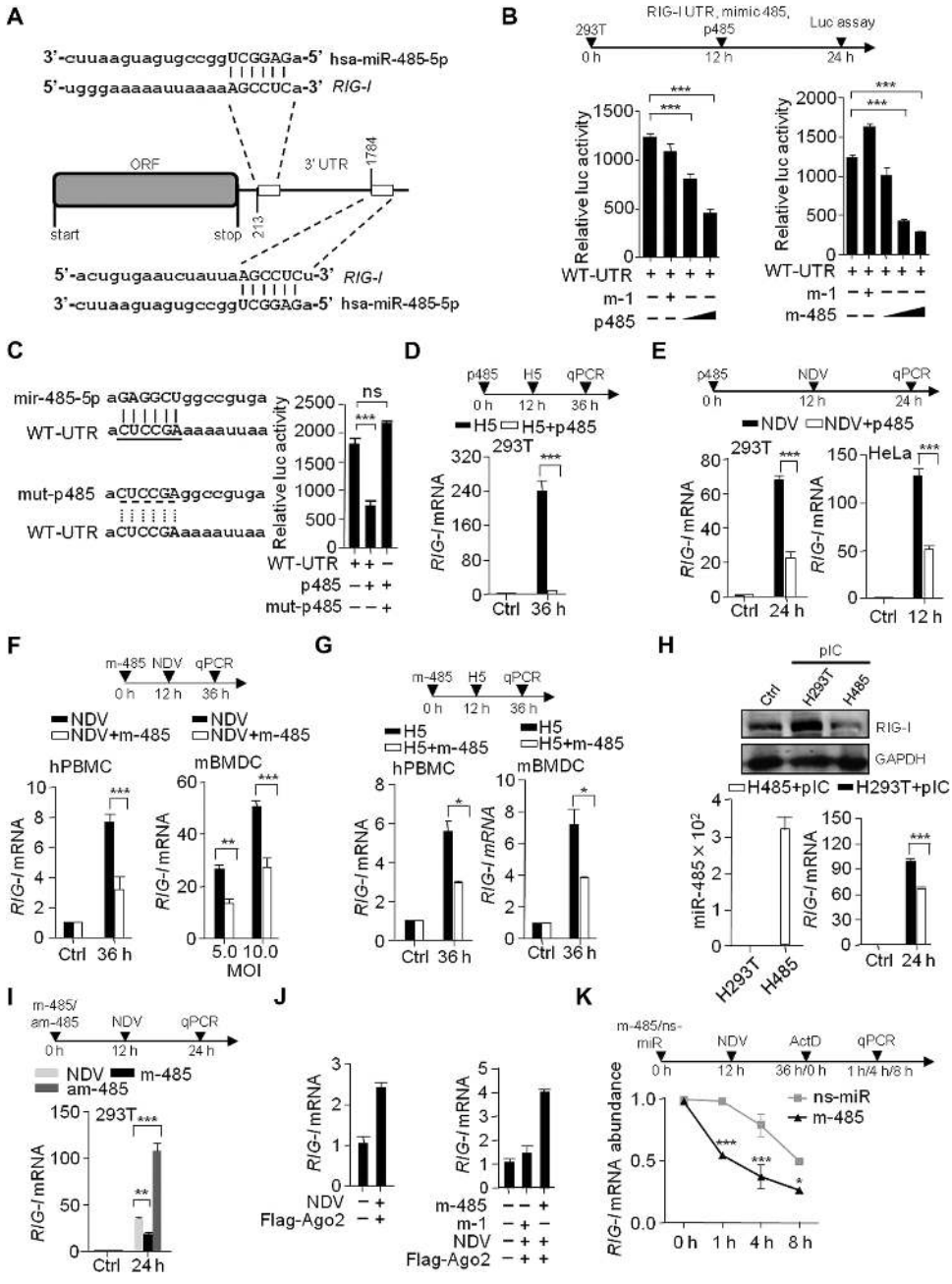

Fig. 2. miR-485 directly targets the conserved 3′UTR of *RIG-I*. (**A**) Seed complementarity of miR-485 with the target site in the 3′UTR of *RIG-I*. ORF, open reading frame. (**B**) HEK 293T cells were transfected at the indicated times with 50 ng of pRL-TK, 100 ng of full-length wild-type (WT) 3′UTR, together with 250 or 500 ng of the plasmid encoding miR-485 (p485; left) or with 25 nM miR-485 mimic (m-485; right) as well as with the appropriate controls. The cells were then lysed and subjected to luciferase assays as described earlier. (**C**) Left: Depiction of the mutations made in the seed sequence of miR-485 to generate mut-p485. Right: HEK 293T cells were transfected with the indicated combinations of WT RIG-I UTR, p485, and mut-p485. Twenty-four hours later, the cells were lysed and subjected to luciferase assays. (**D** to **G**) Quantification of the relative abundance of *RIG-I* mRNA in HEK 293T cells (D and E, left), HeLa cells (E, right), human PBMCs (F), and mouse BMDCs (F) that were transfected with 2 μg of p485 (D and E) or 100 nM miR-485 mimic (F and G) before being infected for the indicated times with H5N1 virus (D and G) or NDV (E and F) at an MOI of 1. (**H**) Left: Quantification of the relative abundance of miR-485 in parental HEK 293T cells and in HEK 293T cells stably expressing miR-485 (H485 cells). HEK 293T (H293T) and H485 cells were transfected with poly(I:C) (5 μg/ml) before being subjected to Western blotting analysis of the relative abundance of RIG-I protein (top) and qRT-PCR analysis of the abundance of *RIG-I* (right). (**I**) Quantification of the abundance of *RIG-I* mRNA in HEK 293T cells that were transfected with the miR-485 mimic or with anti–miR-485 (am-485) before being infected for the indicated times with NDV at an MOI of 1. (**J**) HEK 293T cells were left untransfected or were transfected with the plasmid encoding Flag-Ago2 in the absence (left) or presence (right) of the miR-485 or the miR-1 (m-1) mimic before being subjected to NDV infection at an MOI of 1 for 24 hours. Cell lysates were then subjected to RNA immunoprecipitation with an anti-Flag antibody, and then the relative abundances of *RIG-I* mRNA in the immunoprecipitates were determined by qRT-PCR analysis. (**K**) Quantification of the relative amounts of *RIG-I* mRNA in HEK 293T cells that were infected for 24 hours with NDV at an MOI of 1 and then were left untreated or were treated with actinomycin D (10 μg/ml) for the indicated times. Data are means ± SEM of triplicate samples from a single experiment and are representative of three (B to I and K) or two (J) independent experiments. ***$P < 0.001$ and **$P < 0.01$ by one-way analysis of variance (ANOVA). ns, not significant.

experiment and quantified the *RIG-I* transcripts associated with Ago2, a major protein involved in the RNA-induced silencing complex (RISC). To this end, Flag-tagged Ago2 (Flag-Ago2) was overexpressed in HEK 293T cells, which were then infected with NDV at an MOI of 1 for 12 hours. The amount of *RIG-I* transcripts that coimmunoprecipitated with endogenous miR-485 were then quantified. We found that the abundance of *RIG-I* mRNA was greater in cells overexpressing Flag-Ago2 than in control cells, which suggests that Ago2 facilitates the binding of miR-485 directly to RIG-I (Fig. 2J, left, and fig. S4H). Similar results were obtained by cotransfecting HEK 293T cells with the miR-485 mimic and plasmid encoding Flag-Ago2 and then infecting the cells with NDV at an MOI of 1 for 12 hours (Fig. 2J, right). To understand the mechanism by which miR-485 mediated the suppression of *RIG-I* expression, we transfected HEK 293T cells with the miR-485 mimic or the miR-1 mimic, infected the cells with

NDV for 24 hours, and then treated the cells with actinomycin D, an inhibitor of transcription. We observed that the turnover of *RIG-I* mRNA was enhanced in the presence of miR-485, which suggests that miR-485 suppressed *RIG-I* expression by degrading its mRNA (Fig. 2K). Together, these results suggest that miR-485 suppressed the expression of *RIG-I* after viral infection by directly binding to its 3′UTR and that suppression was mediated through posttranscriptional silencing by degradation of RIG-I mRNA through the formation of the RISC.

miR-485 suppresses the RIG-I–dependent expression of type I and type III IFNs

To further verify the effect of miR-485 on signaling downstream of RIG-I, we examined the expression of genes encoding the type I and type III IFNs in the presence of miR-485. The overexpression of miR-485 inhibited the NDV-induced transcriptional activity of the *IFNα4*, *IFNβ*, *ISRE*, and *IL29* promoters (Fig. 3A and fig. S6A). Through a similar experimental approach, we found that infection with H5N1 and NDV reduced the amounts of the *IFNα*, *IFNβ*, *IP10*, and *IL29* mRNAs in the presence of miR-485 in HEK 293T cells, human SAECs, human PBMCs, mouse BMDCs, and HeLa cells (Fig. 3, B to F, and fig. S6, B to D). Furthermore, H485 cells exhibited a marked reduction in *IFNβ* and *IP10* mRNA abundances after transfection with poly(I:C) (fig. S6E). In addition, miR-485 inhibited the secretion of IP-10 protein by HEK 293T cells infected with increasing amounts of NDV (Fig. 3G). Similar results were obtained in the presence of the miR-485 mimic, whereas anti–miR-485 enhanced the expression of *IFNβ*, *IP10*, and *IL29* in HEK 293T cells (Fig. 3H); however, anti–miR-125a, anti–miR-146a, and anti–miR-205 had no effect on *IFNβ* mRNA abundance in HEK 293T cells after NDV infection (fig. S6F). Together, these results suggest the miR-485 causes a marked decrease in the RIG-I–dependent expression of the genes encoding type I and type III IFNs.

miR-485 dampens the RIG-I–dependent inflammatory response

After viral infection, RLR signaling activates the transcription factor NF-κB, which in turn stimulates the production of inflammatory cytokines. To further study the regulation of the inflammatory response by miR-485, we overexpressed miR-485 in HEK 293T cells and quantified the transcriptional activity of the NF-κB response element. We found that miR-485 substantially reduced the NDV-induced activity of the NF-κB response element (Fig. 4A). We also observed a marked reduction in *IL6* mRNA abundance in miR-485–overexpressing human SAECs and HEK 293T cells that were infected with the H5N1 virus (Fig. 4, B and C). In addition, the NDV-induced expression of *IL6* was substantially reduced in HEK 293T or HeLa cells overexpressing miR-485 (Fig. 4D). Furthermore, the amount of IL-6 protein that was secreted by HEK 293T cells in response to infection with different amounts of NDV was reduced in the presence of miR-485

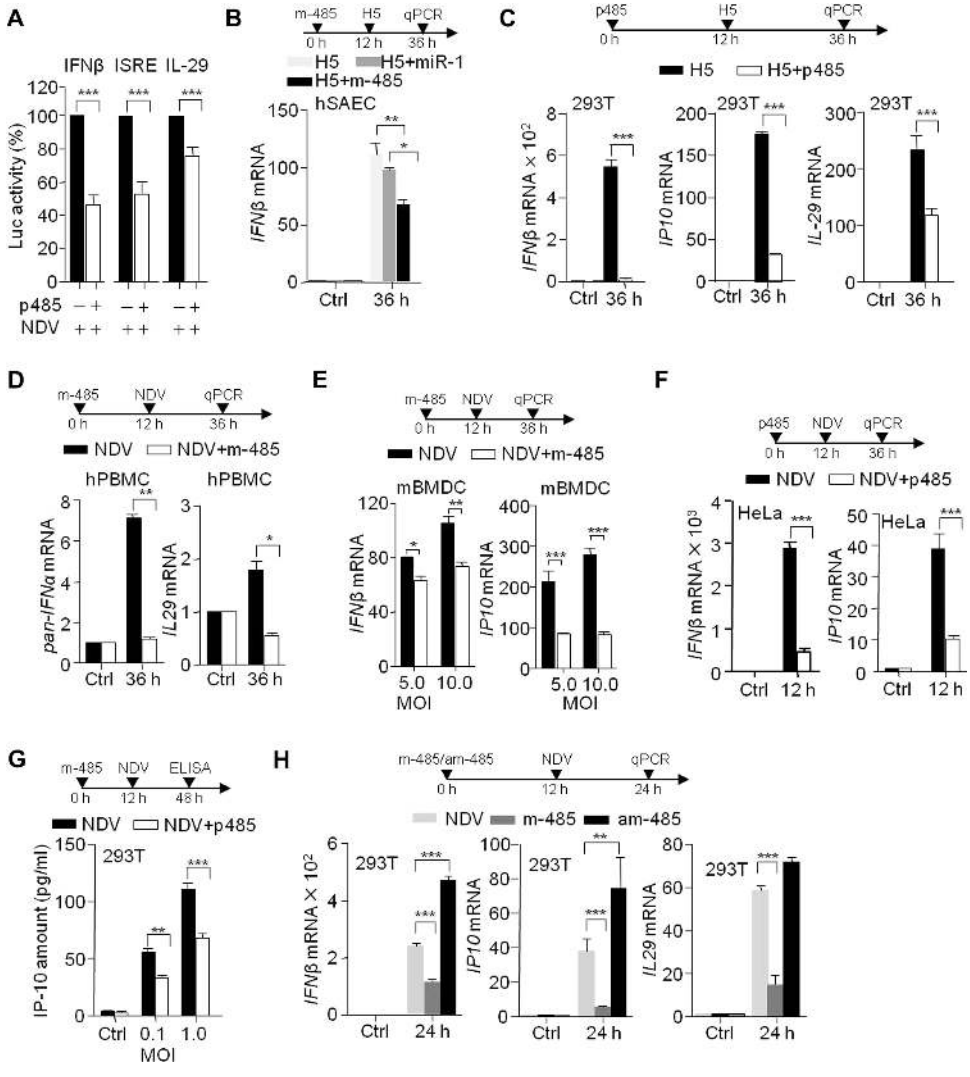

Fig. 3. miR-485 inhibits the virus-induced expression of type I and type III IFNs. (**A**) HEK 293T cells transfected with or without miR-485 and with the indicated luciferase reporters for ISRE, IFN-β, and IL-29 were infected for 24 hours with NDV at an MOI of 1 before being analyzed by luciferase assays as described earlier. (**B** to **H**) Quantification of the abundances of *IFNβ* (B, C, E, F, and H), *IP10* (C, H, E, and F), *IFNα* (D), and *IL29* (C, D, and H) mRNAs in human SAECs (B), HEK 293T cells (C, G, and H), human PBMCs (D), mouse BMDCs (E), and HeLa cells (F) that were transfected with p485 (C and F), the miR-485 mimic (B, D, E, and H), or anti–miR-485 (H) and then were infected for the indicated times with H5N1 (B and C) or NDV (D to F and H) at an MOI of 1. (G) HEK 293T cells were left untransfected or were transfected with p485 before being infected with NDV at an MOI of 0.1 or 1. Twenty-four hours after infection, the amounts of IP-10 protein secreted into the cell culture medium were determined by enzyme-linked immunosorbent assay (ELISA). Data in all panels are means ± SEM of triplicate samples from a single experiment and are representative of three independent experiments. ***$P < 0.001$ and **$P < 0.01$ by one-way ANOVA.

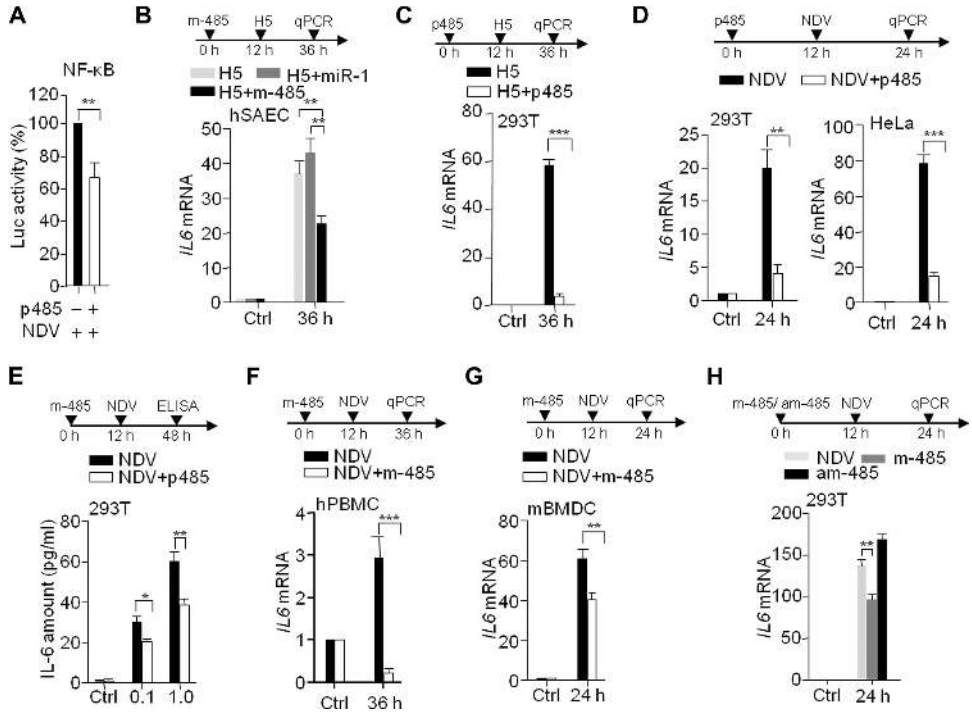

Fig. 4. miR-485 inhibits virus-induced inflammatory responses. (A) HEK 293T cells transfected with the NF-κB reporter with or without miR-485 were then infected with NDV at an MOI of 1. Thirty hours later, the cells were lysed and subjected to luciferase assays. (B to D) Quantification of the relative abundances of *IL6* mRNA in human SAECs (B), HEK 293T cells (C and D), and HeLa cells (D) transfected with the miR-485 mimic (B) or p485 (C and D) and then infected for the indicated times with H5N1 virus (B and C) or NDV (D) at an MOI of 1. (E) HEK 293T cells were left untransfected or were transfected with p485 before being infected for the indicated times with NDV at an MOI of 0.1 or 1. The amounts of IL-6 secreted into the cell culture medium were then determined by ELISA. (F to H) Quantification of the relative abundances of *IL6* mRNA in human PBMCs (F), mouse BMDCs (G), and HEK 293T cells (H) that were left untransfected or were transfected with the miR-485 mimic or anti–miR-485, as indicated, before being infected for the indicated times with NDV at an MOI of 1. Data are means ± SEM of triplicate samples from a single experiment and are representative of three (A to E and H) or two (F and G) independent experiments. $^{***}P < 0.001$ and $^{**}P < 0.01$ by one-way ANOVA.

(Fig. 4E). Similar results were observed in experiments in which human PBMCs and mouse BMDCs were transfected with the miR-485 mimic and then infected with NDV (Fig. 4, F and G). Furthermore, miR-485 suppressed the expression of *IL6* in NDV-infected HEK 293T cells, whereas anti–miR-485 modestly enhanced the expression of *IL6* under similar conditions (Fig. 4H). Together, these results suggest that miR-485 suppresses the inflammatory response downstream of RIG-I.

miR-485 overexpression enhances NDV replication and differentially regulates H5N1 replication

To investigate the physiological role of miR-485 in RNA virus replication, we tested whether the suppression of the antiviral response increased viral replication. To this end, we infected HEK 293T cells with NDV at an MOI of 1 in the presence of p485 and then quantified viral load. Viral RNA quantified by measuring the expression of the gene encoding polymerase L of NDV (hereafter referred as NDV RNA) was substantially increased in abundance in infected cells in the presence of miR-485 (Fig. 5A). Similarly, the miR-485 mimic increased the amount of viral RNA in infected cells, whereas anti–miR-485 markedly decreased the amount of viral RNA compared to that in untransfected control cells or in cells transfected with the control m-1 miRNA (Fig. 5B). However, anti–miR-125a, anti–miR-205, and anti–miR-146a did not cause a substantial change in viral RNA abundance in infected cells (fig. S7A). In addition, we observed an increase in the intracellular virus load in cells transfected with the miR-485 mimic compared to that in cells transfected with the control m-1 miRNA (Fig. 5, C and D). However, the abundance of RIG-I protein was decreased in cells expressing miR-485 (Fig. 5E and fig. S7B). Similar results were obtained from experiments in which human PBMCs and mouse BMDCs were infected with NDV in the presence of the miR-485 mimic (Fig. 5, F and G).

We unexpectedly observed a marked decrease in the viral load, as determined by quantification of the abundance of H5N1 *nucleoprotein* (*NP*) RNA in miR-485–overexpressing human PBMCs that were infected with H5N1 at a higher MOI of 5.0 (Fig. 5H). Ectopic expression of miR-485 in A549 cells resulted in a similar reduction in the replication of the H5N1 virus at a higher MOI of 5.0 (Fig. 5I). In addition, the expression of anti–miR-485 resulted in enhanced H5N1 replication in human PBMCs (fig. S7C). To further investigate this phenomenon, we overexpressed p485 in HEK 293T cells and then infected the cells with H5N1 virus at an MOI of 1 or 5 for 12 or 24 hours and then quantified the viral load. When the cells were infected with virus at a lower MOI, the viral load was markedly increased 12 hours after infection (Fig. 5J, left); however, the viral load was substantially reduced at 24 hours after infection in the presence of miR-485 (Fig. 5J, right). Cells infected with virus at an MOI of 5 showed a marked reduction in viral load at 12 and 24 hours after infection in the presence of miR-485 (Fig. 5K). In addition, a similar phenomenon was observed in experiments in which the live intracellular viral population was estimated by flow cytometric analysis with an anti-NP antibody (Fig. 5L). Together, these results suggest that the differential regulation of NDV and H5N1 by miR-485 is dependent on viral load.

miR-485 bispecifically targets the *PB1* gene of H5N1 and host gene RIG-I

Our previous observation prompted us to investigate the molecular mechanism behind the differential regulation of H5N1 infection by miR-485. We examined whether the single-stranded RNA genome of H5N1 contained any target sites for miR-485. Using the RegRNA and ViTa databases, we scanned for miR-485 target sites in all eight segments of the H5N1 genome. One predominant target site was found to be present in the segment encoding for the RNA-directed RNA polymerase catalytic subunit PB1. The secondary structure of this interaction predicted by the RNA Hybrid software was stable and showed a high mean free energy

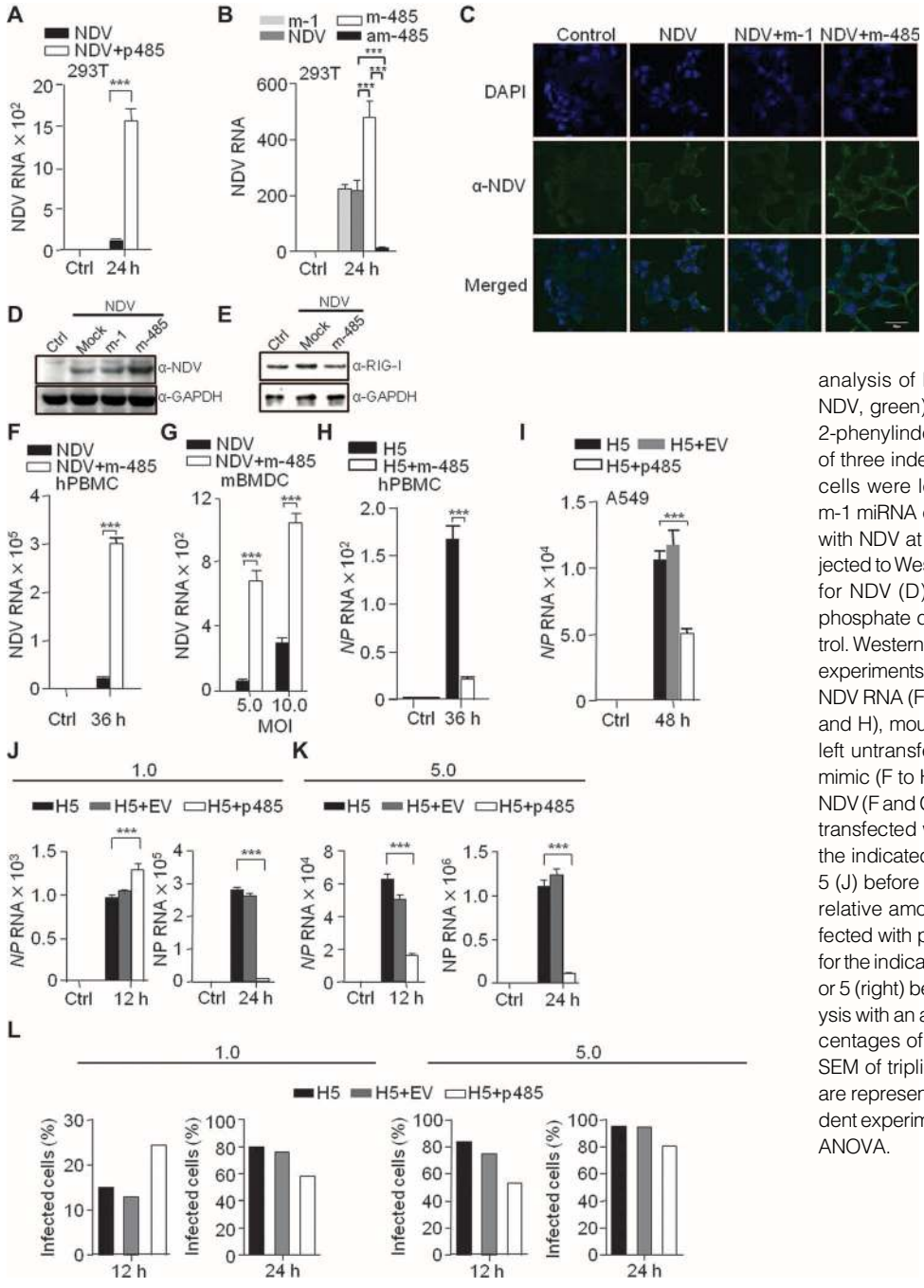

Fig. 5. miR-485 overexpression enhances NDV replication and differentially regulates H5N1 replication. (**A** and **B**) HEK 293T cells transfected with p485 (A) or with the miR-485 mimic, anti–miR-485, or m-1 miRNA (B) were infected for the indicated times with NDV at an MOI of 1 before being subjected to qRT-PCR analysis to determine the relative amounts of NDV RNA. (**C**) HEK 293T cells transfected with the miR-1 or miR-485 mimics were then infected for 24 hours with NDV at an MOI of 1 before being subjected to confocal microscopic analysis of NDV particles with anti-NDV antiserum (α-NDV, green). Nuclei were visualized with 4′,6-diamidino-2-phenylindole (DAPI; blue). Images are representative of three independent experiments. (**D** and **E**) HEK 293T cells were left untransfected or were transfected with m-1 miRNA or the miR-485 mimic and then were infected with NDV at an MOI of 1 for 24 hours before being subjected to Western blotting analysis with antibodies specific for NDV (D) or RIG-I (E). GAPDH (glyceraldehyde-3-phosphate dehydrogenase) was used as a loading control. Western blots are representative of three independent experiments. (**F** to **I**) Quantification of the abundances of NDV RNA (F and G) and *NP* RNA (H) in human PBMCs (F and H), mouse BMDCs (G), and A549 cells (I) that were left untransfected or were transfected with the miR-485 mimic (F to H) or with p485 (I) before being infected with NDV (F and G) or H5N1 (H and I). (**J** and **K**) HEK 293T cells transfected with p485 or empty vector were infected for the indicated times with H5N1 virus at an MOI of 1 (I) or 5 (J) before being subjected to qRT-PCR analysis of the relative amounts of *NP* RNA. (**L**) HEK 293T cells transfected with p485 or empty vector (EV) were then infected for the indicated times with H5N1 virus at and MOI of 1 (left) or 5 (right) before being subjected to flow cytometric analysis with an anti-NP antibody to determine the relative percentages of cells that were infected. Data are means ± SEM of triplicate samples from a single experiment and are representative of three (A to I) or two (J to L) independent experiments. ***$P < 0.001$ and **$P < 0.01$ by one-way ANOVA.

(-24 kcal mol^{-1}) (Fig. 6A). Note that the target site of miR-485 in H5N1 is conserved across various HA subtypes isolated from geographically distinct regions at different time periods (Fig. 6B). To test whether miR-485 targeted *PB1*, we subcloned H5N1 *PB1* into a luciferase reporter plasmid. Through luciferase reporter assays, we found that the luciferase activity in cells expressing the *PB1* reporter was decreased in the presence of miR-485, whereas a reporter based on a mutant *PB1* lacking the miR-485 target site did not exhibit inhibition of luciferase activity (Fig. 6C).

To further elucidate the mechanism underlying the differential regulation of RNA viruses by miR-485, we infected HEK 293T cells with H5N1 virus at an MOI of 1 or 5 and then used RNA immunoprecipitation to analyze the amounts of *PB1* or *RIG-I* transcripts that were bound to miR-485 (Fig. 6D). The amount of *PB1* mRNA bound to endogenous miR-485 was substantially increased in cells infected at a higher MOI (Fig. 6E, left). Similarly, we found that there was an increase in the amount of *PB1* mRNA in infected cells expressing the miR-485 mimic (Fig. 6E, right). Our earlier data suggested that miR-485 bound directly to the 3′UTR of the *RIG-I* transcript. Therefore, we investigated the bispecificity of miR-485 toward both *RIG-I* and H5N1 *PB1*. We found that endogenous miR-485 targeted *RIG-I* mRNAs in HEK 293T cells infected at a lower

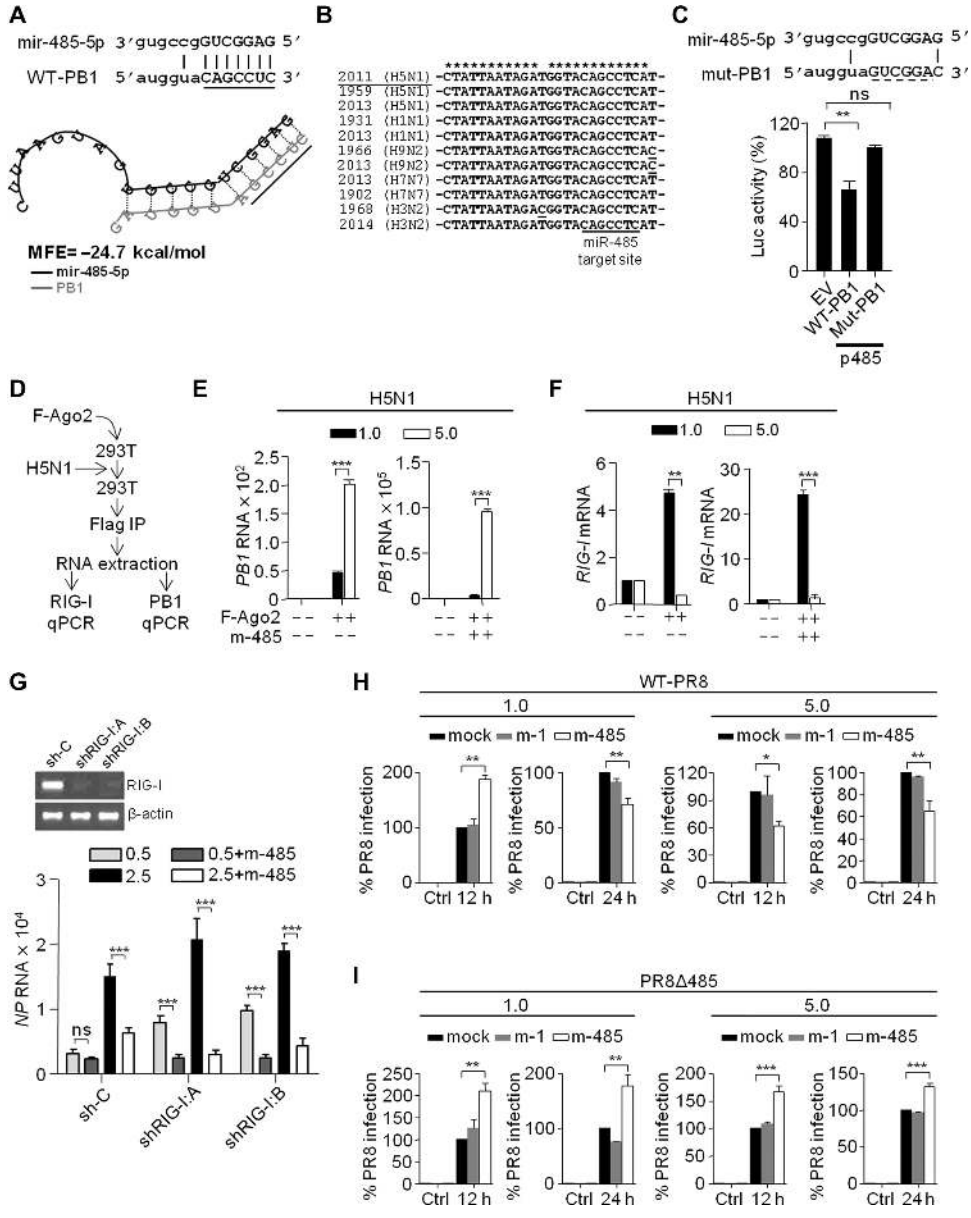

Fig. 6. miR-485 bispecifically targets H5N1 *PB1* and the 3′UTR of *RIG-I*. (**A**) Prediction of the miR-485–binding site in the *PB1* gene of H5N1 and the thermodynamics of the interactions between miR-485 and *PB1*. (**B**) Multiple sequence alignment of the region surrounding the target site of *PB1* across the different strains of IAV generated with ClustalW. (**C**) HEK 293T cells were transfected with 50 ng of pRL-TK and 100 ng of either WT-PB1 or mut-PB1 together with 500 ng of p485 and the appropriate controls. Thirty hours after transfection, the cells were lysed and subjected to luciferase assays. (**D**) Schematic for the RNA immunoprecipitation assay. (**E** and **F**) HEK 293T cells were left untransfected or were transfected with plasmid encoding Flag-Ago2 (F-Agos) in the absence (left) or presence (right) of the miR-485 mimic and then were infected with H5N1 virus at an MOI of 1 (left) or 5 (right). Twenty-four hours after infection, the cells were subjected to RNA immunoprecipitation with anti-Flag antibody and qRT-PCR analysis to determine the relative amounts of *PB1* mRNA (E) and *RIG-I* mRNA (F) that were precipitated. (**G**) HEK 293T cells stably expressing control shRNA, shRIG-I:A, or shRIG-I:B were left untransfected or were transfected with the miR-485 mimic before being infected for 36 hours with H5N1 at an MOI of 0.5 or 2.5. Cells were then analyzed by qRT-PCR to determine the relative amounts of *RIG-I* mRNA. Top: PCR gel showing expression of *RIG-I* mRNA. (**H** and **I**) HEK 293T cells were mock-treated or were transfected with the miR-1 or miR-485 mimics before being infected for the indicated times with WT-PR8 virus (H) or PR8Δ485 mutant virus at an MOI of 1 (left) or 5 (right). The percentages of cells that were infected by virus were determined by considering the abundance of *NP* RNA in the mock-treated cells as 100%. Data are means ± SEM of triplicate samples from a single experiment and are representative of three (C) or two (E to I) independent experiments. ***$P < 0.001$ and **$P < 0.01$ by one-way ANOVA.

MOI; however, in cells infected at a higher MOI, the abundance of *RIG-I* mRNA was reduced (Fig. 6F, left). Similar results were observed in HEK 293T cells overexpressing miR-485 (Fig. 6F, right). To further identify the mechanism underlying the dose-dependent bispecificity of miR-485, we generated stable HEK 293T cell lines in which *RIG-I* expression was knocked down with two specific commercially available short hairpin RNA (shRNA) constructs. The expression of *RIG-I* was markedly reduced in these cell lines compared to that in control shRNA–treated cells (Fig. 6G, top). The control shRNA cells and the RIG-I knockdown cells were infected with H5N1 virus at an MOI of 0.5 or 2.5 for 36 hours in the absence or presence of miR-485. We did not observe any substantial reduction in viral load in the presence of miR-485 in control shRNA cells infected with a low MOI of virus (Fig. 6G, bottom). In contrast, *RIG-I* knockdown cells infected at a low MOI showed a substantial reduction in viral load in the presence of miR-485. When infected at higher MOIs, both the control cells and the *RIG-I* knockdown cells showed a substantial reduction in H5N1 replication in the presence of miR-485 (Fig. 6G, bottom).

Finally, to demonstrate the bispecificity of miR-485 for the 3′UTRs of *RIG-I* and *PB1*, we used the reverse genetics system of PR8/H1N1. The reverse genetics system consists of eight constructs containing the cloned complementary DNAs (cDNAs) representing the eight segments of IAV. These constructs generate progeny virions after transfection of HEK 293T cells. To determine the targeting of *PB1* by miR-485, we mutated the miR-485–binding site in the *PB1* construct by site-directed mutagenesis and generated the wild-type PR8 and mutant PR8/H1N1 (PR8Δ485) viruses. We transfected HEK 293T cells with the miR-485 mimic and then

infected the cells with the wild-type and mutant viruses at MOIs of 1.0 or 5.0 for 12 or 24 hours and quantified the abundance of *NP* RNA to determine viral load. The viral load in mock-treated cells infected at both MOIs was considered as 100% infection. In the case of the wild-type virus, we observed a similar dose-dependent effect of miR-485 on viral load as that exhibited by the H5N1 virus (Fig. 6H). However, replication of the mutant virus lacking the miR-485–binding site was not suppressed in the presence of miR-485 in cells infected at either a lower or a higher MOI (Fig. 6I). Together, these results suggest that miR-485 binds directly to H5N1 *PB1* through a conserved site. The target of miR-485 changes from *RIG-I* to *PB1*, depending on the magnitude of the viral infection. This target switching helps to tune the activation of the innate antiviral responses up to low influenza virus infection.

DISCUSSION

RLR signaling plays a pivotal role in sensing RNA viruses and eliciting a potent antiviral immune response. Various mechanisms regulating RLR signaling that lead to an optimum innate antiviral response have been characterized (*24*–*26*). Here, we propose a model for the posttranscriptional regulation of *RIG-I*. First, we demonstrated that miR-485 directly bound to the 3′UTR of *RIG-I* mRNA and subsequently reduced the abundances of RIG-I mRNA and protein. Second, this interaction substantially reduced the antiviral response, thereby promoting viral replication. Third, we demonstrated that miR-485 targeted the catalytic site in the polymerase PB1 of IAV. Finally, we showed that RIG-I and PB1 switched as being targets of miR-485 in a dose- and viral load–dependent manner during H5N1 infection. These findings not only describe the roles of miRNAs in the regulation of RIG-I but also suggest a previously uncharacterized mechanism for the miRNA-mediated restriction of influenza virus replication.

RIG-I, a cytosolic PRR, senses dsRNA from viruses such as influenza virus, Sendai virus (SeV), and vesicular stomatitis virus (VSV) to induce antiviral signaling. Given the critical function of RIG-I in antiviral innate immunity, it also plays an important role in fine-tuning antiviral responses by undergoing posttranslational modifications that regulate the antiviral cascade (*25*–*27*). There is growing evidence for the miRNA-mediated suppression by viruses of innate antiviral signaling to evade the immune response (*28*, *29*). Both SeV and VSV induce the expression of *mir-4661* in various cell types to directly target *IFNα* mRNA, thereby inhibiting host antiviral innate immune responses (*30*). Similarly, different subtypes of influenza viruses, including A/Udorn/72 and A/WSN/33, specifically induce the expression of various miRNAs, such as miR-7, miR-132, miR-146a, miR-187, miR-200c, and miR-1275, in airway epithelial cells to reduce the abundances of antiviral signaling proteins, such as IRAK1 (interleukin-1 receptor–associated kinase 1) and MAPK3 (mitogen-activated protein kinase 3) (*15*, *16*). Our microarray profiling and in silico screening identified the induction of *mir-485* expression by the RNA viruses NDV and H5N1 in a number of primary cells and various cell lines, including human SAECs and human PBMCs. Previously, miR-485 was reported to play a pivotal role in synaptic plasticity and neurite growth, and it is essential for hippocampal development (*31*, *32*). In addition, miR-485 results in hypertriglycemia by inhibiting the expression of *APOA* (apolipoprotein A) (*33*). Here, we showed that miR-485 directly targeted RIG-I and suppressed innate antiviral responses, leading to enhanced NDV replication.

Influenza virus infection is sensed by TLR3, TLR7, TLR8, RIG-I, and several members of the NLR (NOD-like receptor) family to stimulate appropriate innate and adaptive immune responses (*20*, *34*). Among these sensors, RIG-I plays a pivotal role in the generation of type I IFN–dependent antiviral responses against influenza viruses (*35*–*37*). The segmented genome of IAV bestows on it a distinct ability to undergo genomic recombination to produce different subtypes with altered host specificity and infectivity (*38*). Changes occurring mainly in the genes encoding HA, NA, and the polymerase subunit (PB1) enable the virus to pose a pandemic threat. PB1 serves as a key component of the viral RNP and has RNA-dependent RNA polymerase activity (*39*). Such variations in the sequences encoding PB1 have been implicated in increased pathogenicity and altered host transmission (*40*–*42*). Here, we found that miR-485 specifically targeted the *PB1* gene of H5N1 by direct binding and by reducing its expression, thereby suppressing viral replication. Note that miR-485 targets the catalytic site in the *PB1* gene of H5N1, which is conserved in the other HA subtypes, further illustrating the potential role of miR-485 in inhibiting a wide spectrum of IAVs. Furthermore, the *PB1* gene of IAV contains an alternate ORF that encodes the PB1-F2 protein, which induces cell death and inhibits antiviral signaling by targeting IPS-1 (*43*). Therefore, the direct binding of miR-485 to PB1 may lead to the inhibition of PB1-F2 production, which would further reduce the immune suppression mediated by IAV.

Our results suggest that miR-485 bispecifically targets both RIG-I and PB1 of H5N1 to maintain homeostasis and suppress IAV replication (Fig. 7, A and B). We demonstrated the dose-dependent targeting of *RIG-I* and *PB1* by miR-485 through various experiments, such as RNA immunoprecipitation, knockdown of RIG-I, and the generation of a strain of IAV that was devoid of the miR-485 seed sequence. In cells infected with viruses at lower MOIs, miR-485 targeted RIG-I to dampen the antiviral

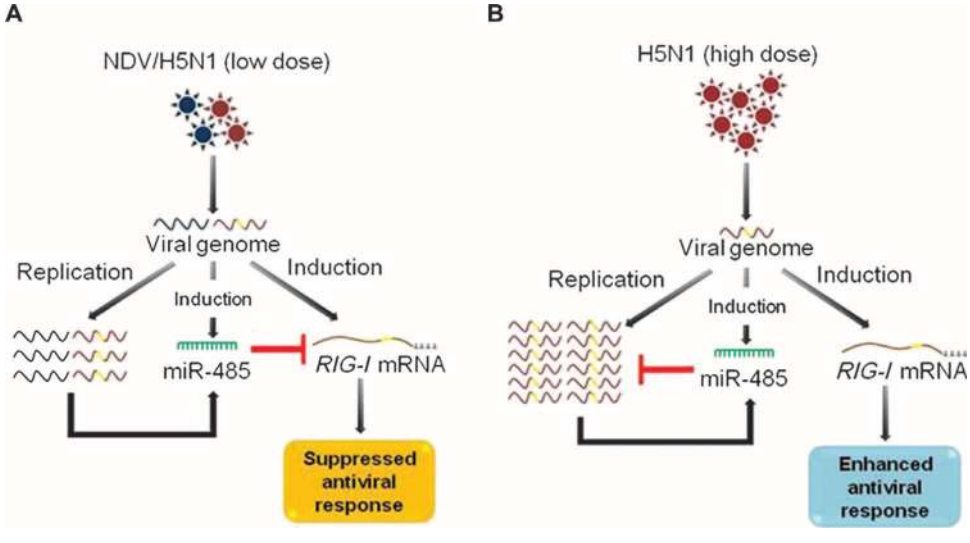

Fig. 7. Bispecific targeting of the 3′UTR of *RIG-I* and *PB1* by miR-485. (A) Model showing the targeting of *RIG-I* by miR-485 and the subsequent effects on antiviral responses and the replication of NDV and H5N1 when present at low viral titers. (B) Model showing the targeting of H5N1 *PB1* by miR-485 and the subsequent effects on antiviral responses and H5N1 replication at high viral titers.

response. This alleviation of RIG-I is an important aspect of the fine-tuning of innate antiviral responses implemented by miRNAs. If the infection intensifies because of an increased viral burden, miR-485 switches to targeting the H5N1 PB1 to inhibit viral replication. Currently, miRNA-based antiviral strategies have been developed for hepatitis C virus infections (*44*–*46*); however, such strategies have not been successfully applied against IAV infections. Stable analogs of miR-485 could be used to treat various types of IAV infections in humans and animals because miR-485 targets the conserved catalytic site in the polymerase *PB1* gene. In summary, we identified miR-485 as a posttranscriptional regulator of *RIG-I* and H5N1 *PB1* expression in a bispecific manner, thereby providing an additional layer of complexity to the regulation of antiviral signaling and the restriction of viral replication through the use of noncoding RNA.

MATERIALS AND METHODS

Profiling of miRNAs

Total RNA was harvested from cells with TRIzol (Invitrogen) according to the manufacturer's protocol. A total of 5 μg of RNA from different samples was subjected to miRNA array analysis with the Affymetrix GeneChip miRNA 4.0 Array. The abundances of miRNAs were detected in viral infected cells and normalized compared to those in uninfected control cells. *P* values were calculated by one-way ANOVA with a *P* value cutoff of 0.05.

In silico analysis for miRNA target gene prediction

Our in silico analysis was based on target site conservation, secondary structure stability, and the thermodynamics of the miRNA-mRNA interaction. To screen the miRNAs obtained from the profiling data, we used TargetScan, DIANA MicroT, and miRanda to identify in the UCSC genome browser those conserved sites in the 3′UTRs of candidate genes encoding cytosolic antiviral sensors. We selected miRNAs that were predicted by the maximum number of programs in common. To determine thermodynamic interactions and secondary structure stability, we analyzed the genes with the PITA and RNA hybrid databases. All of the analysis was performed by taking into account the best optimum scores of each program.

Plasmids and miRNA mimics and inhibitors

The miR-485 mimic (Invitrogen) or a nonspecific miRNA control (miR-1) was used according to the manufacturer's instructions (Applied Biosystems). The miR-485 inhibitor (anti–miR-485) (Invitrogen) was used to inhibit *mir-485* expression in transfected cells. The cDNA encoding the 3′-UTR of *RIG-I* was retrieved from the UCSC gene sorter and was subcloned into the pMIR-REPORT luciferase vector flanked by Hind III sites. Constructs encoding miR-485 were generated by PCR amplification of sequences from genomic DNA. These amplified sequences were then subcloned into the pMIR-REPORT luciferase vector between the Bam HI and Hind III sites after the removal of the luciferase-encoding sequence. A total of 1.8 kb of sequence upstream of the *mir-485* gene was retrieved from the UCSC genome browser. This sequence was amplified by PCR from genomic DNA and was subcloned into the pGL3 basic vector between the Bam HI and Hind III sites. About 800 base pairs of the H5N1-PB1 gene sequence containing the miR-485 target site was amplified by PCR from H5N1 RNA and subcloned into the pMIR-REPORT luciferase vector between the Spe I and Hind III sites. Mutations in the miR-485 construct, in the *PB1* of H5N1 cloned in the reporter plasmid used in the luciferase reporter experiments, and in the *PB1* of PR8/H1N1 used to generate the PR8Δ485 viruses were generated by PCR-based site-directed mutagenesis. The sequence of *PB1* of H5N1 (A/duck/India/02CA10/2011) used in the luciferase experiments was changed from 5′-CAGCCTC-3′ to 5′-GTCGGAG-3′. The sequence of the *mir-485* construct used in the luciferase experiment was changed from 5′-GAGGCT-3′ to 5′-CTCCGA-3′, and the sequence of PB1 of PR8/H1N1 used to generate PR8Δ485 was changed from 5′-CTGCATC-3′ to 5′-GTCGGAC-3′.

Cells, viruses, and reagents

HEK 293T, A549, and MCF7 cells were cultured in Dulbecco's modified Eagle's medium (DMEM) supplemented with 10% fetal bovine serum (FBS) and 1% penicillin-streptomycin. THP1 cells were pretreated with PMA (phorbol 12-myristate 13-acetate) (10 ng/ml), cultured in RPM1 supplemented with 10% FBS, and maintained at 37°C and 5% CO_2. Human PBMCs were isolated from whole blood as previously described (*47*). Mouse BMDCs were prepared as previously described (*48*). Human SAECs were purchased and maintained in the prescribed growth medium (Lonza). The HPAI A/duck/India/02CA10/2011 (H5N1) and NDV LaSota viral stocks were inoculated into specific pathogen–free 10-day-old embryonated eggs. A single virus stock was used for all experiments. All experiments were performed in biosafety level 3 laboratories (BSL3) at the National Institute of High Security Animal Diseases (NIHSAD). The cells were infected in serum-free DMEM with the HPAI and NDV viruses at the MOIs indicated in the figure legends. After 60 min, the cells were washed with phosphate-buffered saline (PBS) and then were resuspended in DMEM, 10% FBS. Transfection of cells with DNA was performed with Lipofectamine 2000 (Invitrogen) according to the manufacturer's protocol. Poly(I:C) (Invivogen) was mixed with Lipofectamine 2000 before being used to transfect cells. DMEM, FBS, Opti-MEM, penicillin-streptomycin, RPMI, and Lipofectamine 2000 were purchased from Invitrogen. Murine GM-CSF was purchased from GenScript.

Generation of HEK 293T cells expressing miR-485 or RIG-I–specific shRNA

To generate HEK 293T cells stably expressing miR-485, we transfected the cells with 30 μg of the p485 construct with the Gene Pulser Xcell electroporation system (Bio-Rad Laboratories) according to the manufacturer's instructions. The cells were cultured in DMEM, 10% FBS containing puromycin (0.5 μg/ml). The efficiency of expression of miR-485 in stable cells was determined by quantifying the abundance of miR-485 by qRT-PCR analysis. For shRNA-mediated stable knockdown of RIG-I, shRNA clones specifically targeting human RIG-I and scrambled shRNA were obtained from Mission shRNA (Sigma-Aldrich). HEK 293T cells were stably transfected with 30 μg of the shRNA clones and were cultured by selection in DMEM, 10% FBS containing puromycin (0.7 μg/ml). The efficiency with which the shRNA clones decreased the abundance of *RIG-I* mRNA was determined by semiquantitative PCR.

Generation of the A/PR8/H1N1 virus

The wild-type and mutant A/PR8/H1N1 viruses were generated from eight plasmids as described previously (*49*, *50*). Briefly, the eight plasmids were transfected in a coculture of HEK 293T cells and Madin-Darby canine kidney (MDCK) cells cultured in DMEM supplemented with 10% FBS. After 48 hours, the medium was collected and overlaid on MDCK cells for further amplification of the viral titers.

Electroporation or transfection of cells with miRNA mimics

For electroporation of human PBMCs and mouse BMDCs, 1×10^6 cells were suspended in Opti-MEM (Invitrogen) containing 200 mM mirVana miRNA mimics (Ambion). The cells were pulsed twice with 1000 V for

0.5 ms with a pulse interval of 5 s with the Gene Pulser Xcell electroporation system. The cells were then transferred to RPMI (for human PBMCs) or DMEM (for mouse BMDCs) supplemented with 10% FBS (*51*). SAECs were transfected with Lipofectamine 2000 according to the manufacturer's instructions.

Dual luciferase assays

HEK 293T cells (5×10^4) were seeded into a 24-well plate and transiently transfected with 50 ng of the transfection control pRL-TK plasmid and 100 ng of the luciferase reporter plasmid together with 500 ng of the various expression plasmids or an empty plasmid as a control. The cells were lysed at 24 to 36 hours after transfection, and the luciferase activity in total cell lysates was measured with Glomax (Promega).

Enzyme-linked immunosorbent assay

HEK 293T cells were transiently transfected with p485 and then were infected with H5N1 or NDV viruses. The culture media were harvested 36 to 40 hours after infection and were analyzed by specific ELISA kits (Becton Dickinson) according to the manufacturer's instructions to determine the amounts of IP-10 and IL-6 that were secreted by the cells.

Quantitative real-time reverse transcription PCR

Total RNA was extracted with the Purelink RNA Mini Kit (Ambion) and used to synthesize cDNA with the iScript cDNA Synthesis Kit (Bio-Rad) according to the manufacturer's protocol. Gene expression was measured by quantitative real-time PCR using gene-specific primers and SYBR Green (Roche). For quantification of the abundances of *mir-146a, mir-205, mir-125a,* and *mir-485*, real-time PCR analysis was performed with the TaqMan Universal PCR Master Mix (Applied Biosystems) and the individual TaqMan miRNA assays. The Taqman U6 assay was used as a reference control.

Flow cytometric analysis

Cells were fixed in 4% paraformaldehyde (PFA), permeabilized with 0.1% Triton X-100, and then incubated with anti-NP antibody and Alexa Fluor 488–conjugated donkey anti-mouse secondary antibody. The cells were analyzed with a FACSAria III flow cytometer (Becton Dickinson), and the data were analyzed with FlowJo software.

Confocal microscopy

Cells were fixed with 4% PFA for 20 min at 4°C; permeabilized with 0.05% Triton X-100 in PBS for 10 min at room temperature; blocked with bovine serum albumin (5 mg/ml) in PBS, 0.04% Tween 20 for 30 min; and incubated for 1 hour with the relevant primary antibodies diluted in blocking buffer. The cells were then washed three times with PBS and incubated for 1 hour with the appropriate secondary antibodies at room temperature. Nuclei were stained with DAPI, and the cells were then analyzed with an LSM 780 confocal laser microscope (Carl Zeiss). The images were analyzed using ImageJ processing software.

RNA immunoprecipitations

RNA immunoprecipitations were performed as described previously (*52*, *53*). The pIRESneo-Flag/HA Ago2 plasmid was a gift from T. Tuschl (Addgene plasmid #10822). Briefly, HEK 293T cells were lysed in 0.5% NP-40, 150 mM KCl, 25 mM tris-glycine (pH 7.5) and incubated with M2 Flag affinity beads overnight. The lysate was then washed with 300 mM NaCl, 50 mM tris-glycine (pH 7.5), 5 mM $MgCl_2$, and 0.05% NP-40. The extraction of RNA from the immunoprecipitated RNPs was performed with the Trizol reagent according to the manufacturer's protocol.

Western blotting analysis

After cells were infected with NDV, lysates were collected and subjected to Western blotting analysis as described previously (*54*). Anti–RIG-I antibody was obtained from Sigma-Aldrich, and horseradish peroxidase–conjugated anti-rabbit antibody was obtained from GE Healthcare. Anti-NP antibody specific for influenza virus was obtained from CSIRO Australia, and antiserum against NDV was generated from chicken at the NIHSAD.

Statistical analysis

All experiments were performed together with the appropriate controls, which are indicated as untreated cells (Ctrl) or as being transfected with the transfection reagent alone (Mock). Experiments were performed with duplicate or triplicate samples per experiment and were performed at least three times independently. GraphPad Prism 5.0 (GraphPad Software) was used for statistical analysis. Differences between two groups were compared by an unpaired, two-tailed Student's *t* test, whereas differences between three groups or more were compared by ANOVA with the Newman-Keuls test. Differences were considered to be statistically significant when $P < 0.05$. Statistical significance in the figures is indicated as follows: $***P < 0.001$, $**P < 0.01$, $*P < 0.05$; ns, not significant.

SUPPLEMENTARY MATERIALS

www.sciencesignaling.org/cgi/content/full/8/406/ra126/DC1

Fig. S1. Kinetics of viral infections of human cells.
Fig. S2. Kinetics of the effects of transfection of various human cells with poly(I:C).
Fig. S3. miR-485 is increased in abundance in HEK 293T cells after viral infection.
Fig. S4. miR-485 suppresses the expression of *RIG-I*.
Fig. S5. Analysis of the miR-485–mediated regulation of *MDA5* expression.
Fig. S6. miR-485 suppresses the virus-induced expression of IFN-encoding genes and promotes NDV replication.
Fig. S7. An miR-485 inhibitor differentially regulates the replication of H5N1 and NDV.
Table S1. miRNA expression profile in HEK 293T cells infected with NDV.

REFERENCES AND NOTES

1. O. Takeuchi, S. Akira, Pattern recognition receptors and inflammation. *Cell* **140**, 805–820 (2010).
2. R. Barbalat, S. E. Ewald, M. L. Mouchess, G. M. Barton, Nucleic acid recognition by the innate immune system. *Annu. Rev. Immunol.* **29**, 185–214 (2011).
3. H. Kato, K. Takahasi, T. Fujita, RIG-I-like receptors: Cytoplasmic sensors for non-self RNA. *Immunol. Rev.* **243**, 91–98 (2011).
4. D. Goubau, S. Deddouche, C. Reis e Sousa, Cytosolic sensing of viruses. *Immunity* **38**, 855–869 (2013).
5. J. Wu, Z. J. Chen, Innate immune sensing and signaling of cytosolic nucleic acids. *Annu. Rev. Immunol.* **32**, 461–488 (2014).
6. A. G. Bowie, L. Unterholzner, Viral evasion and subversion of pattern-recognition receptor signalling. *Nat. Rev. Immunol.* **8**, 911–922 (2008).
7. J. R. Patel, A. García-Sastre, Activation and regulation of pathogen sensor RIG-I. *Cytokine Growth Factor Rev.* **25**, 513–523 (2014).
8. S. Reikine, J. B. Nguyen, Y. Modis, Pattern recognition and signaling mechanisms of RIG-I and MDA5. *Front. Immunol.* **5**, 342 (2014).
9. J. Hou, P. Wang, L. Lin, X. Liu, F. Ma, H. An, Z. Wang, X. Cao, MicroRNA-146a feedback inhibits RIG-I-dependent Type I IFN production in macrophages by targeting TRAF6, IRAK1, and IRAK2. *J. Immunol.* **183**, 2150–2158 (2009).
10. L. A. O'Neill, F. J. Sheedy, C. E. McCoy, MicroRNAs: The fine-tuners of Toll-like receptor signalling. *Nat. Rev. Immunol.* **11**, 163–175 (2011).
11. Y. Li, X. Shi, MicroRNAs in the regulation of TLR and RIG-I pathways. *Cell. Mol. Immunol.* **10**, 65–71 (2013).
12. D. P. Bartel, MicroRNAs: Genomics, biogenesis, mechanism, and function. *Cell* **116**, 281–297 (2004).
13. L. He, G. J. Hannon, MicroRNAs: Small RNAs with a big role in gene regulation. *Nat. Rev. Genet.* **5**, 522–531 (2004).
14. A. S. Flynt, E. C. Lai, Biological principles of microRNA-mediated regulation: Shared themes amid diversity. *Nat. Rev. Genet.* **9**, 831–842 (2008).
15. W. A. Buggele, K. E. Johnson, C. M. Horvath, Influenza A virus infection of human respiratory cells induces primary microRNA expression. *J. Biol. Chem.* **287**, 31027–31040 (2012).

16. W. A. Buggele, K. E. Krause, C. M. Horvath, Small RNA profiling of influenza A virus-infected cells identifies miR-449b as a regulator of histone deacetylase 1 and interferon beta. *PLOS One* **8**, e76560 (2013).
17. M. L. Yarbrough, K. Zhang, R. Sakthivel, C. V. Forst, B. A. Posner, G. N. Barber, M. A. White, B. M. A. Fontoura, Primate-specific miR-576-3p sets host defense signalling threshold. *Nat. Commun.* **5**, 4963 (2014).
18. L. Song, H. Liu, S. Gao, W. Jiang, W. Huang, Cellular microRNAs inhibit replication of the H1N1 influenza A virus in infected cells. *J. Virol.* **84**, 8849–8860 (2010).
19. Z. Zheng, X. Ke, M. Wang, S. He, Q. Li, C. Zheng, Z. Zhang, Y. Liu, H. Wang, Human microRNA hsa-miR-296-5p suppresses enterovirus 71 replication by targeting the viral genome. *J. Virol.* **87**, 5645–5656 (2013).
20. A. Iwasaki, P. S. Pillai, Innate immunity to influenza virus infection. *Nat. Rev. Immunol.* **14**, 315–328 (2014).
21. I. Ramos, A. Fernandez-Sesma, Innate immunity to H5N1 influenza viruses in humans. *Viruses* **4**, 3363–3388 (2012).
22. J.-S. Yoo, H. Kato, T. Fujita, Sensing viral invasion by RIG-I like receptors. *Curr. Opin. Microbiol.* **20**, 131–138 (2014).
23. B. N. Fields, D. M. Knipe, P. M. Howley, *Fields Virology* (Wolters Kluwer Health/Lippincott Williams & Wilkins, Philadelphia, ed. 5, 2007).
24. J. J. Chiang, M. E. Davis, M. U. Gack, Regulation of RIG-I-like receptor signaling by host and viral proteins. *Cytokine Growth Factor Rev.* **25**, 491–505 (2014).
25. E. Wies, M. K. Wang, N. P. Maharaj, K. Chen, S. Zhou, R. W. Finberg, M. U. Gack, Dephosphorylation of the RNA sensors RIG-I and MDA5 by the phosphatase PP1 is essential for innate immune signaling. *Immunity* **38**, 437–449 (2013).
26. W. Zeng, L. Sun, X. Jiang, X. Chen, F. Hou, A. Adhikari, M. Xu, Z. J. Chen, Reconstitution of the RIG-I pathway reveals a signaling role of unanchored polyubiquitin chains in innate immunity. *Cell* **141**, 315–330 (2010).
27. M. U. Gack, Y. C. Shin, C.-H. Joo, T. Urano, C. Liang, L. Sun, O. Takeuchi, S. Akira, Z. Chen, S. Inoue, J. U. Jung, TRIM25 RING-finger E3 ubiquitin ligase is essential for RIG-I-mediated antiviral activity. *Nature* **446**, 916–920 (2007).
28. O. Haller, G. Kochs, F. Weber, The interferon response circuit: Induction and suppression by pathogenic viruses. *Virology* **344**, 119–130 (2006).
29. S. Schutz, P. Sarnow, Interaction of viruses with the mammalian RNA interference pathway. *Virology* **344**, 151–157 (2006).
30. Y. Li, X. Fan, X. He, H. Sun, Z. Zou, H. Yuan, H. Xu, C. Wang, X. Shi, MicroRNA-466l inhibits antiviral innate immune response by targeting interferon-alpha. *Cell. Mol. Immunol.* **9**, 497–502 (2012).
31. J. E. Cohen, P. R. Lee, S. Chen, W. Li, R. D. Fields, MicroRNA regulation of homeostatic synaptic plasticity. *Proc. Natl. Acad. Sci. U.S.A.* **108**, 11650–11655 (2011).
32. J. E. Cohen, P. R. Lee, R. D. Fields, Systematic identification of 3′-UTR regulatory elements in activity-dependent mRNA stability in hippocampal neurons. *Philos. Trans. R. Soc. Lond. B Biol. Sci.* **369**, 20130509 (2014).
33. C. Caussy, S. Charrière, C. Marçais, M. Di Filippo, A. Sassolas, M. Delay, V. Euthine, A. Jalabert, E. Lefai, S. Rome, P. Moulin, An *APOA5* 3′ UTR variant associated with plasma triglycerides triggers *APOA5* downregulation by creating a functional miR-485-5p binding site. *Am. J. Hum. Genet.* **94**, 129–134 (2014).
34. C. Lupfer, P. G. Thomas, T. D. Kanneganti, Nucleotide oligomerization and binding domain 2-dependent dendritic cell activation is necessary for innate immunity and optimal $CD8^+$ T cell responses to influenza A virus infection. *J. Virol.* **88**, 8946–8955 (2014).
35. M. Schlee, A. Roth, V. Hornung, C. A. Hagmann, V. Wimmenauer, W. Barchet, C. Coch, M. Janke, A. Mihailovic, G. Wardle, S. Juranek, H. Kato, T. Kawai, H. Poeck, K. A. Fitzgerald, O. Takeuchi, S. Akira, T. Tuschl, E. Latz, J. Ludwig, G. Hartmann, Recognition of 5′ triphosphate by RIG-I helicase requires short blunt double-stranded RNA as contained in panhandle of negative-strand virus. *Immunity* **31**, 25–34 (2009).
36. J. Rehwinkel, C. P. Tan, D. Goubau, O. Schulz, A. Pichlmair, K. Bier, N. Robb, F. Vreede, W. Barclay, E. Fodor, C. Reis e Sousa, RIG-I detects viral genomic RNA during negative-strand RNA virus infection. *Cell* **140**, 397–408 (2010).
37. M. Weber, A. Gawanbacht, M. Habjan, A. Rang, C. Borner, A. M. Schmidt, S. Veitinger, R. Jacob, S. Devignot, G. Kochs, A. García-Sastre, F. Weber, Incoming RNA virus nucleocapsids containing a 5′-triphosphorylated genome activate RIG-I and antiviral signaling. *Cell Host Microbe* **13**, 336–346 (2013).
38. S. Herfst, M. Imai, Y. Kawaoka, R. A. M. Fouchier, Avian influenza virus transmission to mammals. *Curr. Top. Microbiol. Immunol.* **385**, 137–155 (2014).
39. A. J. Eisfeld, G. Neumann, Y. Kawaoka, At the centre: Influenza A virus ribonucleoproteins. *Nat. Rev. Microbiol.* **13**, 28–41 (2015).
40. Y. Suzuki, Y. Uchida, T. Tanikawa, N. Maeda, N. Takemae, T. Saito, Amino acid substitutions in PB1 of avian influenza viruses influence pathogenicity and transmissibility in chickens. *J. Virol.* **88**, 11130–11139 (2014).
41. E. J. A. Schrauwen, M. de Graaf, S. Herfst, G. F. Rimmelzwaan, A. D. M. E. Osterhaus, R. A. M. Fouchier, Determinants of virulence of influenza A virus. *Eur. J. Clin. Microbiol. Infect. Dis.* **33**, 479–490 (2014).
42. T. Watanabe, G. Zhong, C. A. Russell, N. Nakajima, M. Hatta, A. Hanson, R. McBride, D. F. Burke, K. Takahashi, S. Fukuyama, Y. Tomita, E. A. Maher, S. Watanabe, M. Imai, G. Neumann, H. Hasegawa, J. C. Paulson, D. J. Smith, Y. Kawaoka, Circulating avian influenza viruses closely related to the 1918 virus have pandemic potential. *Cell Host Microbe* **15**, 692–705 (2014).
43. Z. T. Varga, A. Grant, B. Manicassamy, P. Palese, Influenza virus protein PB1-F2 inhibits the induction of type I interferon by binding to MAVS and decreasing mitochondrial membrane potential. *J. Virol.* **86**, 8359–8366 (2012).
44. H. L. A. Janssen, H. W. Reesink, E. J. Lawitz, S. Zeuzem, M. Rodriguez-Torres, K. Patel, A. J. van der Meer, A. K. Patick, A. Chen, Y. Zhou, R. Persson, B. D. King, S. Kauppinen, A. A. Levin, M. R. Hodges, Treatment of HCV infection by targeting microRNA. *N. Engl. J. Med.* **368**, 1685–1694 (2013).
45. Y. Stram, L. Kuzntzova, Inhibition of viruses by RNA interference. *Virus Genes* **32**, 299–306 (2006).
46. D. Grimm, All for one, one for all: New combinatorial RNAi therapies combat hepatitis C virus evolution. *Mol. Ther.* **20**, 1661–1663 (2012).
47. D. Bharti, A. Kumar, R. S. Mahla, S. Kumar, H. Ingle, H. Shankar, B. Joshi, A. A. Raut, H. Kumar, The role of TLR9 polymorphism in susceptibility to pulmonary tuberculosis. *Immunogenetics* **66**, 675–681 (2014).
48. H. Kumar, T. Kawai, H. Kato, S. Sato, K. Takahashi, C. Coban, M. Yamamoto, S. Uematsu, K. J. Ishii, O. Takeuchi, S. Akira, Essential role of IPS-1 in innate immune responses against RNA viruses. *J. Exp. Med.* **203**, 1795–1803 (2006).
49. E. de Wit, M. I. J. Spronken, T. M. Bestebroer, G. F. Rimmelzwaan, A. D. M. E. Osterhaus, R. A. M. Fouchier, Efficient generation and growth of influenza virus A/PR/8/34 from eight cDNA fragments. *Virus Res.* **103**, 155–161 (2004).
50. L. Martinez-Sobrido, A. García-Sastre, Generation of recombinant influenza virus from plasmid DNA. *J. Vis. Exp.*, e2057 (2010).
51. A. Nikonov, T. Mölder, R. Sikut, K. Kiiver, A. Männik, U. Toots, A. Lulla, V. Lulla, A. Utt, A. Merits, M. Ustav, RIG-I and MDA-5 detection of viral RNA-dependent RNA polymerase activity restricts positive-strand RNA virus replication. *PLOS Pathog.* **9**, e1003610 (2013).
52. M. Beitzinger, G. Meister, Experimental identification of microRNA targets by immunoprecipitation of Argonaute protein complexes. *Methods Mol. Biol.* **732**, 153–167 (2011).
53. G. Meister, M. Landthaler, A. Patkaniowska, Y. Dorsett, G. Teng, T. Tuschl, Human Argonaute2 mediates RNA cleavage targeted by miRNAs and siRNAs. *Mol. Cell* **15**, 185–197 (2004).
54. S. Kumar, H. Ingle, S. Mishra, R. S. Mahla, A. Kumar, T. Kawai, S. Akira, A. Takaoka, A. A. Raut, H. Kumar, IPS-1 differentially induces *TRAIL*, *BCL2*, *BIRC3* and *PRKCE* in type I interferons-dependent and -independent anticancer activity. *Cell Death Dis.* **6**, e1758 (2015).

Acknowledgments: We thank R. Fouchier for providing the A/PR8/H1N1 reverse genetics system. We thank T. Tuschl for providing the Ago2-Flag construct through Addgene. We thank Indian Institute of Science Education and Research (IISER) Bhopal for providing the Central Instrumentation Facility, and NIHSAD for providing the Advanced Biosafety Level 3 facility. We are grateful to M. Sharma and S. Bhattacharya for technical assistance. We are thankful to S. Banerjee for helping with the statistical analysis. **Funding:** H.I. is supported by the IISER Bhopal institutional fellowship; S.K. is a recipient of a CSIR India Senior research fellowship; H.K. is a recipient of a Ramanujan fellowship provided by the Department of Science and Technology (DST), India. This work was supported by research grant numbers SR/S2/RJN-55/2009 and BT/PR6009/GBD/27/382/2012 from the DST and Department of Biotechnology, Government of India; the IISER Bhopal–IGM Hokkaido University Grant for General Joint Research Program of the Institute for Genetic Medicine, Hokkaido University for 2015; and an Intramural Research Grant of IISER, Bhopal, India, to H.K. **Author contributions:** H.I. and H.K. conceptualized the study and designed the experiments; H.I and S.K. performed the experiments; H.I., S.K., and H.K. analyzed the data; H.I., A.A.R., and H.K. designed the H5N1 experiments; H.I., A.A.R., and A.M. performed the H5N1 experiments; T.K., A.T., and S.A. provided critical reagents; D.D.K. provided the infrastructure; H.I and H.K. wrote the manuscript; and H.K. supervised the entire project. **Competing interests:** The authors declare that they have no competing interests. **Data and materials availability:** The microarray data for miRNA profiling reported in this paper have been deposited in the GenBank database (accession no. GSE65694).

Submitted 9 April 2015
Accepted 18 November 2015
Final Publication 8 December 2015
10.1126/scisignal.aab3183
Citation: H. Ingle, S. Kumar, A. A. Raut, A. Mishra, D. D. Kulkarni, T. Kameyama, A. Takaoka, S. Akira, H. Kumar, The microRNA miR-485 targets host and influenza virus transcripts to regulate antiviral immunity and restrict viral replication. *Sci. Signal.* **8**, ra126 (2015).

The microRNA miR-485 targets host and influenza virus transcripts to regulate antiviral immunity and restrict viral replication

Harshad Ingle, Sushil Kumar, Ashwin Ashok Raut, Anamika Mishra, Diwakar Dattatraya Kulkarni, Takeshi Kameyama, Akinori Takaoka, Shizuo Akira and Himanshu Kumar (December 8, 2015)
Science Signaling **8** (406), ra126. [doi: 10.1126/scisignal.aab3183]

Science Signaling (ISSN 1937-9145) is published weekly, except the last December, by the American Association for the Advancement of Science, 1200 New York Avenue, NW, Washington, DC 20005.